

Meridional structure and future changes of tropopause height and temperature

Shineng Hu¹ | Geoffrey K. Vallis²

¹Scripps Institution of Oceanography,
University of California, San Diego, La
Jolla, California

²Department of Mathematics, University of
Exeter, Exeter, UK

Correspondence

Shineng Hu, Scripps Institution of
Oceanography, University of California, San
Diego, La Jolla, CA.
Email: shineng.hu@gmail.com

Abstract

We use a simple, semianalytic, column model to understand better the meridional structure of the tropopause height and future changes in its height and temperature associated with global warming. The model allows us to separate the effects of tropospheric lapse rate, optical depth, outgoing longwave radiation (OLR), and stratospheric cooling on the tropopause height. When applied locally at each latitudinal band, the model predicts the overall meridional structure of the tropopause height, with a tropical tropopause substantially higher than in higher latitudes and a sharp transition at the edge of the extratropics. The large optical depth of the Tropics, due mainly to the large water-vapour path, is the dominant tropospheric effect producing the higher tropical tropopause, whereas the larger tropical lapse rate actually acts to lower the tropopause height. The dynamical cooling induced by the stratospheric circulation lifts the thermal tropopause in the Tropics further, resulting in it being significantly cooler and higher than in mid- and high-latitudes.

The model quantifies the causes of the tropopause height increase with global warming that is found robustly in climate integrations from the fifth Coupled Model Intercomparison Project (CMIP5). The large spread in the increase rate of tropopause height in the CMIP5 model is captured by the simple model, which attributes the dominant contributions to changes in water-vapour path and lapse rate, with changes in CO₂ concentration and OLR having much smaller direct effects. The CMIP5 models also show a small but robust increase in the tropopause temperature in low latitudes, with a much smaller increase in higher latitudes. We suggest that the tropical increase may be caused at least in part by nongrey effects in the radiative transfer associated with the higher levels of water vapour in the Tropics, with near-constant tropopause temperatures predicted otherwise.

KEYWORDS

climate change, global warming, tropopause

1 | INTRODUCTION

The tropopause is the boundary separating the relatively quiescent stratosphere and relatively active troposphere. The thermal stratification in the stratosphere is constrained

primarily by radiative processes and, to a lesser extent, by the slow large-scale overturning circulation. In contrast, the tropospheric lapse rate is maintained by faster dynamical processes acting on much shorter timescales, such as moist convection in the Tropics and baroclinic eddies in the extratropics

(e.g., Manabe and Strickler, 1964; Held, 1982; Vallis, 2017). The height and temperature of the tropopause control many aspects of the Earth's climate system—for example, the horizontal and vertical scales of baroclinic eddies and the amount of water vapour in the stratosphere, respectively—so that understanding its structure, and whether and how that might change in future, is of fundamental importance.

Various definitions of tropopause height have been proposed, based on, for example, lapse rate, potential vorticity, or the level to which the active circulation reaches, and certainly one definition might be more appropriate than another for any given purpose (World Meteorological Organization, 1957; Danielsen, 1968; Holton *et al.*, 1995; Wilcox *et al.*, 2012). Nevertheless, they all agree on the most prominent feature, namely that the annual-mean zonal-mean tropical tropopause is significantly higher than that over the polar regions (about 16 km versus 8 km), with a fairly sharp transition at the edge of the Hadley Cell as the Tropics transitions to the extratropics (Figure 1a). Our goals in this article are to understand the overall height and meridional structure of tropopause height better, and whether and why the tropopause height and temperature might change in future. The meridional structure is, in fact, quite well simulated by the current generation of climate models, for example those in the CMIP5 archive. However, simulation is not always the same as understanding

and, of perhaps more practical importance, the models in the archive respond in different ways and by different amounts under global warming. Here we will seek to clarify these issues via the construction and use of a relatively simple model that enables us to specifically attribute the meridional structure and temporal changes in tropopause height and temperature to specific changes in lapse rate, optical path, and other parameters.

The basic problem is the determination of the overall height of the tropopause. Radiative balance must be achieved at the top of the atmosphere, and, if the optical thickness is small at the tropopause level and the atmosphere is grey in the infrared, then the temperature of the tropopause can be related to the emitting temperature of the atmosphere, a long-standing and fairly easily derived result (Held, 1982; Vallis, 2017). That radiative constraint has motivated the construction of radiative–convective models for tropopause height in various versions (e.g., Held, 1982; Thuburn and Craig, 1997; 2000; Vallis *et al.*, 2015), and a key step in constructing such models is to suppose that the lapse rate is determined dynamically in the troposphere and radiatively above. Held (1982) assumed a specified outgoing longwave radiation at the top of the atmosphere, thus giving the “radiative constraint”, and argued that the height of the tropopause varies inversely with the tropospheric lapse rate (the TLR, $-dT/dz$), since the tropopause has to shift downward in order to maintain an unchanged emission temperature if the lapse rate increases. In such a model, the tropopause height can be obtained by way of a numerical calculation, and, with further assumptions, an approximate analytic expression can be derived (Vallis *et al.*, 2015). Thuburn and Craig (1997; 2000) constructed a similar radiative–convective model, but with a specified surface temperature rather than outgoing longwave radiation, and investigated the stratospheric influence on the tropopause height; in particular, they found that the height of the tropopause is relatively insensitive to stratospheric ozone but can be modulated by the stratospheric residual circulation, confirmed by their GCM simulations.

Those and other studies have given rise to our basic understanding of the tropopause, but a number of questions remain—for example, what determines the climatological meridional structure of tropopause height? The tropospheric lapse rate is actually greater in the Tropics than in the mid-latitudes (Stone and Carlson, 1979; Mokhov and Akperov, 2006; see figure 15.25 in Vallis, 2017); in low latitudes, the lapse rate is given primarily by the moist adiabatic lapse rate but is also influenced by baroclinic eddies in the mid-latitudes (Juckes, 2000; Schneider, 2004; Zurita-Gotor and Vallis, 2011; 2013). The fact that the tropical tropopause is higher than that in the midlatitudes is then puzzling, because the inverse dependence of tropopause height on lapse rate suggests a lower tropical tropopause. Evidently, other factors play a role in determining the meridional tropospheric structure.

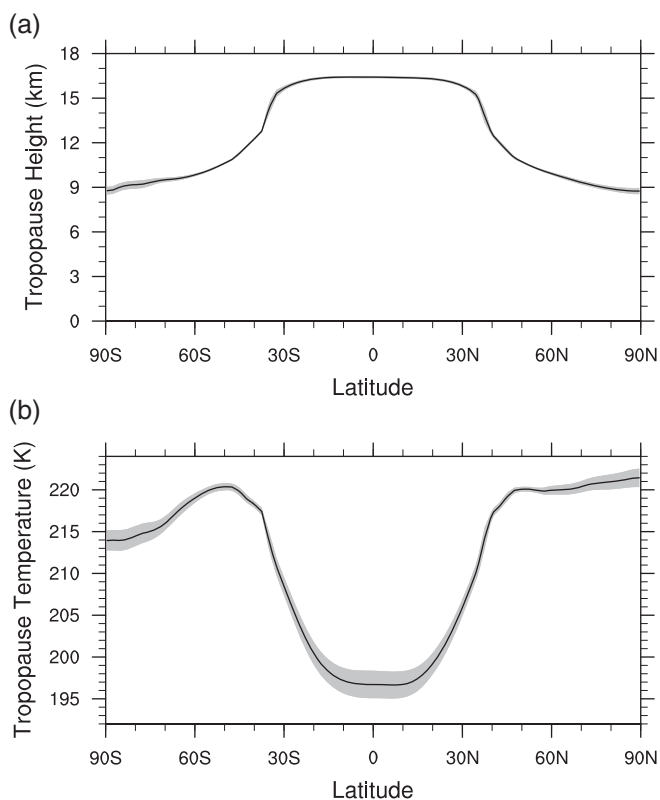


FIGURE 1 (a) Present-day annual-mean zonal-mean tropopause height averaged over the period 1979–2017. The grey shading highlights the interannual variations measured by standard deviation. (b) Same as (a) but for the tropopause temperature. Derived from the NCEP2 product

For example, the abundance of water vapour could potentially give rise to a greater tropopause height, since tropopause height tends to increase with optical thickness to maintain an unchanged emission temperature (an extreme example is Venus, where the tropopause is at about 60 km because of the very large greenhouse effect). To what extent the two effects (lapse rate versus optical depth) cancel each other and how they work together with other controlling factors to shape the meridional structure of tropopause height need to be addressed. Our first goal is to understand that structure.

Our second goal is to understand future changes in tropopause height and temperature with global warming. The increase in tropopause height under greenhouse warming is one of the most robust features of simulations with comprehensive climate models (Lorenz and DeWeaver, 2007; Lu *et al.*, 2008; Vallis *et al.*, 2015), and is consistent with the observed trend over recent decades (Santer *et al.*, 2003). Vallis *et al.* (2015) argue that the twin causes of the tropopause lifting are the reduction in tropospheric lapse rate (because of a change in the moist adiabatic lapse rate) and the increase in optical depth. Even if this is the case, these factors have not been quantified and there is considerable intermodel spread in the CMIP5 results that is not well understood. Changes in tropopause temperature are also not well understood: grey models with an optically thin stratosphere predict an unchanging tropopause temperature (Vallis *et al.*, 2015), but CMIP results show tropopause temperatures increasing (although the increase is smaller than that at the surface).

In order to understand and explain all these phenomena better, we will develop and use a simple column model with minimal physics. The model is not intended to capture all the aspects of atmospheric thermal structure fully; rather, it contains only the essential components that are relevant to the tropopause height and temperature. The model specifies three main parameters, the outgoing longwave radiation, tropospheric lapse rate, and optical depth, with the height and temperature of the tropopause and the surface temperature being predicted by the model. Stratospheric influences from ozone and residual circulation may be added as needed. Using such a model, we can see explicitly which parameters influence the height and temperature of the tropopause, and the cause of their variations with latitude and time. Atmospheric circulation is not incorporated explicitly in the model, except in so far as it is taken into account by the specification of the tropospheric lapse rate that is specified in the model.

We begin in section 2 by briefly describing the main datasets used in this study, including a reanalysis product for the present climate and the CMIP5 model outputs for a future warmer climate. In section 3 we describe the tropopause model and discuss the key assumptions and the model sensitivity. In section 4 we apply the model to understand the meridional structure of tropopause height in the present climate, and in section 5 we discuss the impacts of stratospheric

circulation and ozone heating. In section 6 we look at possible changes in tropopause height associated with global warming. In section 7, we extend the tropopause model to have an infrared window, with implications for future changes in tropopause temperature. We summarize and conclude, and discuss the model limitations, in section 8.

2 | DATA AND METHODS

In this article we will consider only the annual-mean zonal-mean climate states. For the present climate, we use National Centers for Environmental Prediction (NCEP) Reanalysis 2 (hereafter NCEP2) data provided by the National Oceanic and Atmospheric Administration/Oceanic and Atmospheric Research/Earth System Research Laboratory (NOAA/OAR/ESRL) Physical Sciences Division (PSD), Boulder, Colorado, from their website at <https://www.esrl.noaa.gov/psd/>. We define the height of the tropopause using the thermal definition provided by the World Meteorological Organization (WMO). For each latitude, we firstly compute the zonal-mean annual-mean temperature and then identify the lowest level where the lapse rate drops below $2^{\circ}\text{C}/\text{km}$ and remains smaller than $2^{\circ}\text{C}/\text{km}$ within 2 km above. Next, we interpolate the temperature between the tropopause and the surface on to even height levels, and compute the mean tropospheric lapse rate using a linear regression analysis. The present mean state is defined as the long-term average of monthly data over the period 1979–2017.

To study the future warming climate, we use the CMIP5 model outputs for the 1pctCO2 scenario. In this scenario, CO₂ concentration increases steadily by 1% per year (denoted as “1% scenario” hereafter), which corresponds to a quadrupling of CO₂ level by year 140. The whole 140-year period of integration is used for linear trend analysis, and the phrase “change” due to greenhouse warming then refers to the trend multiplied by one century. The tropopause height and the tropospheric lapse rate within each climate model are defined in the same way as for NCEP2. We obtain datasets from 24 general circulation models (GCMs) that match the 140-year requirement and contain all variables needed. The GCMs include ACCESS1-0, ACCESS1-3, CanESM2, CCSM4, CMCC-CM, CNRM-CM5, CNRM-CM5-2, CSIRO-Mk3-6-0, CSIRO-Mk3L-1-2, GFDL-CM3, GISS-E2-H, GISS-E2-R, HadGEM2-ES, Inmcm4, IPSL-CM5A-LR, IPSL-CM5A-MR, IPSL-CM5B-LR, MIROC5, MIROC-ESM, MPI-ESM-MR, MPI-ESM-P, MRI-CGCM3, NorESM1-M, and NorESM1-ME.

3 | A SIMPLE TROPOPAUSE MODEL

We now describe the essential components of a tropopause model based on the one presented in Vallis *et al.* (2015),

which in turn draws from Held (1982) and Thuburn and Craig (2000). Following those studies, we assume an atmosphere that is transparent to solar radiation and grey in the infrared. We will discuss the impact of ozone-induced solar heating in section 5. We write the longwave radiation transfer equations (e.g., Goody, 1964), as

$$\frac{\partial D}{\partial \tau} = B - D, \quad \frac{\partial U}{\partial \tau} = U - B, \quad (1)$$

where D and U are downward and upward infrared irradiance, respectively, and $B = \sigma T^4$ follows the Stefan–Boltzmann law with $\sigma = 5.67 \times 10^{-8} \text{ W/m}^2$. τ is optical depth, increasing downward. At the top of the atmosphere, where $\tau = 0$, we have the upper boundary conditions $D = 0$ and $U = \text{OLR}$ (the outgoing longwave radiation), which we assume is given (or taken from observations).

For ease of calculation, we define two variables, I and J , using linear combinations of U and D , as follows:

$$I = U - D, \quad J = U + D. \quad (2)$$

Equation 1 can thus be rewritten as, equivalently,

$$\frac{\partial I}{\partial \tau} = J - 2B, \quad \frac{\partial J}{\partial \tau} = I. \quad (3)$$

The upper boundary conditions become $I = \text{OLR}$ and $J = \text{OLR}$ at $\tau = 0$.

We assume that the stratosphere is in radiative equilibrium (RE), where the convergence of longwave radiation vanishes. We relax this assumption and discuss the impact of stratospheric dynamical heating in section 5. The stratospheric RE can thus be written as

$$\frac{\partial I}{\partial \tau} = 0 \quad \text{and} \quad \frac{\partial I}{\partial z} = 0. \quad (4)$$

A consequence of this is that, in radiative equilibrium, I is constant in the vertical,

$$I = \text{OLR}. \quad (5)$$

Combining Equations 3 and 5, and the top of atmosphere boundary condition $J = \text{OLR}$, we get

$$J = (\tau + 1)\text{OLR}. \quad (6)$$

Then, based on Equation 2, we can easily derive the expressions for D and U ,

$$D, U = \left(\frac{\tau}{2}, \frac{\tau + 2}{2} \right) \text{OLR}, \quad (7)$$

and from Equations 3 and 4 we see that

$$B = \frac{J}{2} = \left(\frac{\tau + 1}{2} \right) \text{OLR}. \quad (8)$$

Using the Stefan–Boltzmann law, we get the radiative equilibrium temperature profile for the stratosphere,

$$T_{\text{re}} = \left[\left(\frac{\tau + 1}{2\sigma} \right) \text{OLR} \right]^{1/4}. \quad (9)$$

Note that the radiative equilibrium solutions above are determined by OLR and τ only and do not depend on the lower boundary conditions on the ground.

Further, we assume a stratosphere in radiative equilibrium governed by Equation 7 and a uniformly stratified troposphere, separated by a tropopause at $z = H_T$,

$$T(z) = \begin{cases} T_{\text{re}}, & z \geq H_T, \\ T_T + \Gamma(H_T - z), & H_T \geq z \geq 0, \end{cases} \quad (10)$$

where $\Gamma = -dT/dz$ is the tropospheric lapse rate and the tropopause temperature $T_T = T_{\text{re}}|_{z=H_T}$. The lower boundary condition at the surface requires that $U = \sigma T_s^4$ at $z = 0$, where T_s is the surface temperature (that is, no ground temperature jump).

We specify the vertical profile of optical depth as

$$\tau(z) = \tau_{\text{ws}} \exp(-z/H_a) + \tau_{\text{ds}} \exp(-z/H_s), \quad (11)$$

where τ_{ws} and τ_{ds} are the surface optical depths associated with water vapour and dry air, respectively, and H_a and H_s are the scale heights of water vapour and dry air, respectively; in Earth’s atmosphere, they have values of about $H_a = 2 \text{ km}$ and $H_s = 8 \text{ km}$. We assume that atmospheric pressure decreases exponentially with height, $p = p_s \exp(-z/H_s)$, where surface pressure $p_s = 1,000 \text{ hPa}$. Therefore the vertical coordinates of τ , p , and z can be converted.

After specifying OLR, Γ , τ_{ws} , and τ_{ds} , we obtain numerical solutions of tropopause height by iterating over the different values of H_T until the lower boundary condition is matched. (This procedure differs from that of Thuburn and Craig (2000), since we specify the outgoing longwave radiation, not surface temperature.) The model sensitivity to the key variables in the ranges that are relevant to the Earth’s present climate is shown in Figure 2.

When the surface optical depth increases, the emission height increases (to keep the emission temperature constant) and the tropopause must also rise (Figure 2a,c). When tropospheric lapse rate decreases (as it would in a wetter atmosphere), the tropopause height must again increase to keep the emission temperature constant (Figure 2a,c). Finally, for a fixed lapse rate, an increase in outgoing longwave radiation also leads to a higher tropopause (Figure 2b,c). This

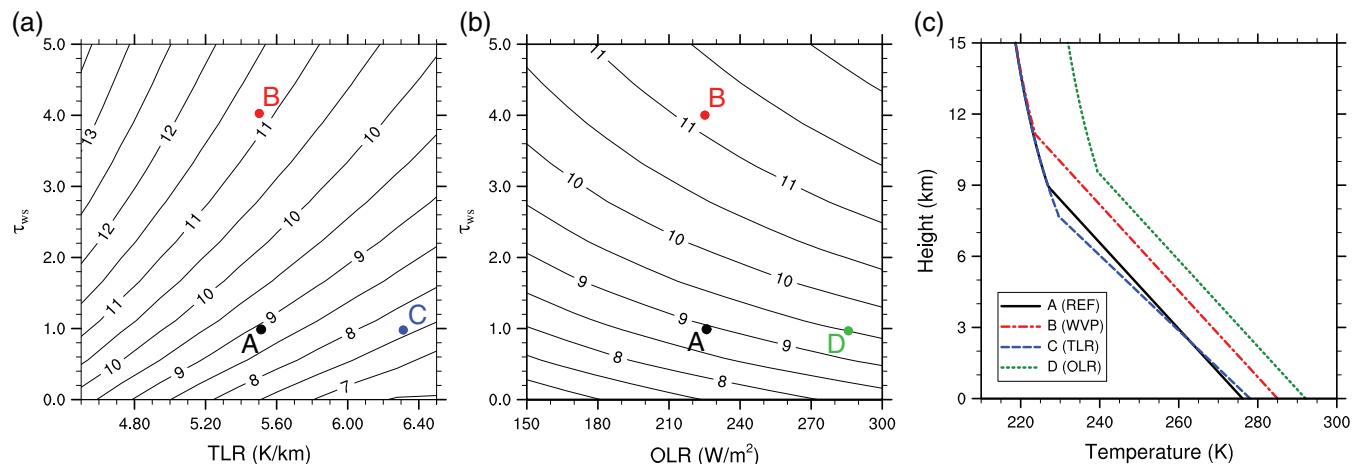


FIGURE 2 Numerical solutions of tropopause height as a function of τ_{ws} and (a) tropospheric lapse rate (TLR) and (b) outgoing longwave radiation (OLR). We set a constant value of $\tau_{ds} = 1$. In (a), we set $OLR = 225 \text{ W/m}^2$. In (b), we set $TLR = 5.5 \text{ K/km}$. (c) Temperature profiles associated with the cases marked in the phase diagrams (panels a and b): Point A is the reference case, while Points B, C, and D refer to the cases with only water-vapour path (or τ_{ws}), tropospheric lapse rate, or outgoing longwave radiation, respectively, having been changed [Colour figure can be viewed at wileyonlinelibrary.com]

result is not quite obvious, since a higher tropopause implies a lower temperature, but a higher outgoing longwave radiation also gives rise to a warmer troposphere as a whole. We note that the direct dependence of tropopause height on outgoing longwave radiation itself is relatively weak.

In some cases, the above model admits an approximate analytic solution (Vallis *et al.*, 2015). If the optical depth varies simply as $\tau(z) = \tau_s \exp(-z/H_a)$ and H_a is much less than the height of the tropopause, so that the optical depth is small in the stratosphere, then we find

$$H_T = \frac{1}{16\Gamma} \left(CT_T + \sqrt{C^2 T_T^2 + 32\Gamma \tau_s H_a T_T} \right), \quad (12)$$

where $C = \log 4 \approx 1.4$, Γ is the lapse rate, T_T is the temperature at the tropopause, τ_s is the surface optical depth, and H_a is the scale height of the main infrared absorber. We will not use Equation 12 for calculations in this article (since more general numerical results are easily obtained), but the equation is instructive in telling us that the tropopause height varies inversely with lapse rate (as expected), and how it increases with surface optical depth, tropopause temperature (and hence OLR), and the scale height of the absorber. Results from Equation 12 are quite similar to those shown in Figure 2, with the dependences in Equation 12 reflected in changes in tropopause height in Figure 2c. Reference to Equation 12 will be useful in interpreting the results throughout the article.

Many restrictive assumptions have been made in our model. We assume an atmosphere that is grey to infrared radiation and transparent to shortwave radiation; the grey assumption is relaxed in section 7.1 and shortwave absorption by ozone is considered in section 5. Also, atmospheric circulation is not simulated explicitly by the model, due to

the column model set-up; the role of stratospheric residual circulation is briefly discussed in section 5 and the potential model improvement to account at least partly for the tropospheric circulation is discussed in section 8. We specify the values of water-vapour path and tropospheric lapse rate and assume that they are independent controlling factors; in the real world, they might be closely related, at least in the deep Tropics, and potential modifications to the model are discussed in section 8. We assume a constant lapse rate in the troposphere, which is likely to be a poor assumption in polar regions, where there may be a low-level inversion.

4 | MERIDIONAL STRUCTURE OF TROPOPAUSE HEIGHT

We now apply the tropopause model to the different latitudinal bands and explore the meridional structure of tropopause height. For optical depth (Equation 11), we assume a fixed $\tau_{ds} = 1$ that does not vary with latitude, and a τ_{ws} that gradually decreases with latitude to mimic the poleward reduction of water-vapour path (denoted WVP). In idealized general circulation models, surface optical depth is often assumed to decrease sinusoidally with latitude (Frierson *et al.*, 2006; O’Gorman and Schneider, 2008). Here, we simply assume that τ_{ws} varies linearly with water-vapour path following $\tau_{ws} = \alpha \text{WVP}$, where $\alpha = 0.1 \text{ mm}^{-1}$. Since the water-vapour path decreases from about 40 mm at the Equator to zero at the poles, the surface optical depth decreases from approximately 5 to 1, similar to the meridional profiles used in those idealized general circulation models (e.g., in Frierson *et al.* (2006), surface optical depth decreases from 6 at the Equator to 1.5 at the poles). The resultant climate has a similar

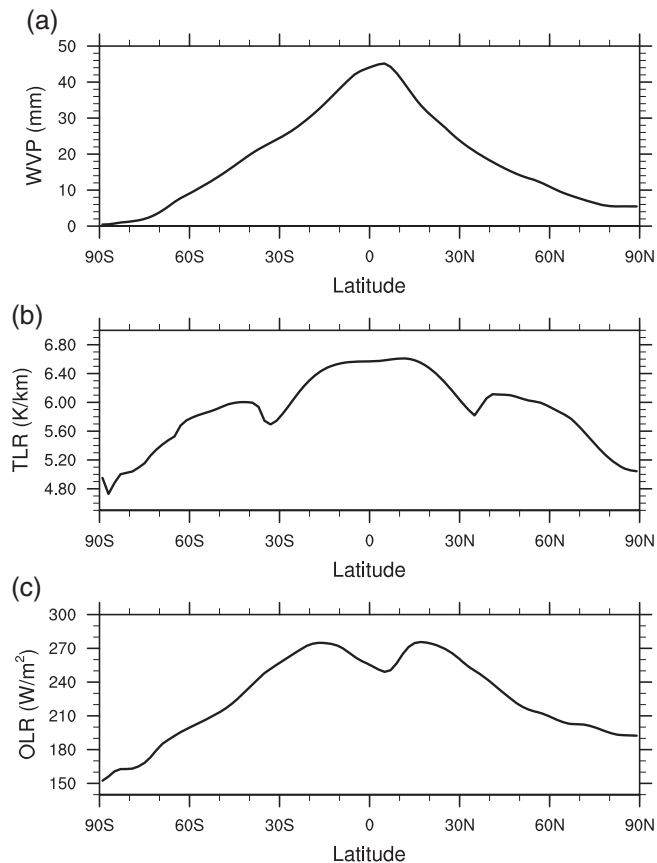


FIGURE 3 Present-day annual-mean zonal-mean (a) water-vapour path (WVP), (b) tropospheric lapse rate (TLR), and (c) outgoing longwave radiation (OLR) as a function of latitude averaged over the period 1979–2017. Derived from the NCEP2 product

meridional structure of surface temperature to the observations with a global mean surface temperature of 15 °C. Note that the meridional heat transport of the atmosphere–ocean system is taken into account by the specification of the outgoing longwave radiation as an upper boundary condition to the model.

The surface optical path τ_s (and so water-vapour content integrated over the depth of the atmosphere), tropospheric lapse rate (i.e., Γ) and outgoing longwave radiation are the three key variables in our model (as can be seen from Equation 12, in which T_T parametrizes the outgoing longwave radiation), and they are all characterized by substantial meridional variations. Figure 3 shows their annual-mean zonal-mean meridional profiles computed from the NCEP2 product. Water-vapour content peaks at the Equator with a maximum value of 40 mm, decreases almost linearly with latitude, and nearly vanishes over the polar regions (Figure 3a). The outgoing longwave radiation decreases poleward as the layers emitting infrared radiation get cooler, and the Equator-to-pole contrast is about 100 W/m² (Figure 3c).

In the tropical atmosphere, horizontal tropospheric temperature gradients are relatively small within 30°S–30°N,

while surface temperature is uniform only in a narrower equatorial band within 15°S–15°N. As a result, the tropospheric lapse rate experiences nonmonotonic changes with latitude: it reaches the highest value of 6.5 K/km following the moist adiabats in the equatorial band, starts to decrease at 15° of latitude, begins to increase at 35° of latitude, and finally decreases towards the poles, where the lowest value of 5 K/km occurs (Figure 3b).

Next we use those three meridional profiles (i.e., water-vapour path, tropospheric lapse rate and outgoing longwave radiation) as inputs for our tropopause model to predict the meridional structure of tropopause height (Figure 4a). To isolate their individual contribution, we conduct three sensitivity cases, where we only allow one of them to vary with latitude while fixing the other two at their global mean values for all latitudes. As noted earlier, tropospheric lapse rate alone leads to a lower tropopause in the Tropics compared with the polar tropopause, which is not in accord with the observations. Even though the inverse relationship between tropospheric lapse rate and tropopause height has been known for a long time (Held, 1982; Thuburn and Craig, 2000; Vallis *et al.*, 2015), this contradiction with the observations has not received much attention and has to be reconciled by other controlling factors. Indeed, we find that the greater water-vapour path (i.e., thicker optical depth) in the Tropics instead results in a much higher tropopause than that over the poles by about 4 km, working against the effect of tropospheric lapse rate. The strong compensation between the tropospheric lapse rate and the water-vapour path in determining the meridional structure of tropopause height, to the best of our knowledge, has not been reported in previous literature. This should not be confused with the compensation between water-vapour feedback and lapse-rate feedback under global warming (Held and Soden, 2000) and, in fact, the latitudinal relationship and the temporal relationship between the two are opposite; from poles to Equator the lapse rate increases as water vapour increases, while under global warming the lapse rate decreases as water vapour increases. The impact of outgoing longwave radiation on the tropopause height is relatively small; a 100 W/m² Equator-to-pole contrast of outgoing longwave radiation only leads to 1 km difference in the tropopause height.

With all the three factors included, the tropopause model is able to produce some aspects of the observed meridional structure of tropopause height, although with various discrepancies (Figure 4). The competing effects of water-vapour path, tropospheric lapse rate and outgoing longwave radiation lead to an almost flat tropopause in the Tropics. The sharp transition of tropopause height occurs at about 35°S (35°N), which results from the nonmonotonic change of tropospheric lapse rate with latitude near the edge of the Tropics (Figure 3b; see our discussion above). Outside the Tropics, the tropopause height generally decreases with latitude except

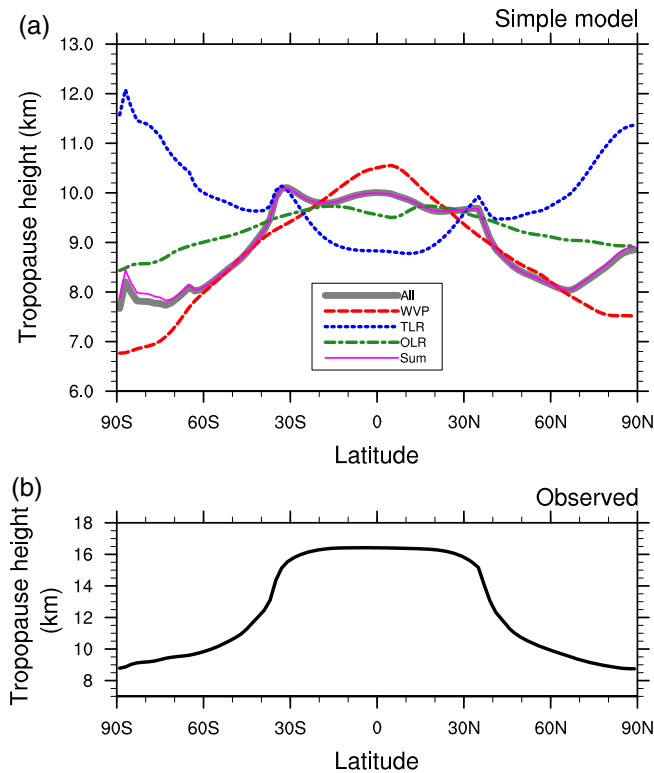


FIGURE 4 (a) The model-predicted tropopause height as a function of latitude using input information from NCEP2. The dashed line corresponds to the model-predicted tropopause height with only the latitude dependence of water-vapour path (WVP), while keeping the other two factors at their global mean values. Similarly, the dotted and dot-dashed lines are for model-predicted tropopause height with only the latitude dependence of tropospheric lapse rate (TLR) or outgoing longwave radiation (OLR), respectively. The thick solid line is for the tropopause height with the latitude dependence of all three factors included, and the thin solid line is the linear sum of the three curves, with an offset for better comparison with the thick grey curve. (b) The annual-mean zonal-mean tropopause height from NCEP2 is shown for comparison [Colour figure can be viewed at wileyonlinelibrary.com]

for the slight reversal poleward of 65°N . All these features resemble those in observations. Still, the Equator-to-pole contrast in tropopause height predicted by the model (2 km) is too small compared with the observations (8 km), and the equatorial tropopause is too warm (Figure 5). In the next section, we will revise the simple model to include the tropical dynamical cooling effects of the stratospheric circulation to account for such discrepancies.

5 | THE ROLE OF STRATOSPHERIC CIRCULATION AND OZONE HEATING

In our model so far, the stratosphere is assumed to be in radiative equilibrium and the absorption of shortwave solar radiation is ignored. In reality, a stratospheric residual circulation and ozone heating are present and important to the

thermal structure of the stratosphere (as is well known, e.g., Thuburn and Craig, 2000; Birner, 2010; Haqq-Misra *et al.*, 2011; Zurita-Gotor and Vallis, 2013; Vallis *et al.*, 2015) and, as we shall see, to the tropopause height. We will start with the role of stratospheric residual circulation, followed by that of ozone heating.

As noted, the Equator-to-pole contrast of tropopause height produced by the model is too small compared with that seen in observations. Moreover, the tropical tropopause is actually significantly colder than the midlatitude and polar tropopause by about 20 K (Figure 1b), and this feature is not captured by the model (Figure 5). Previous studies suggest that the stratospheric circulation that consists of an ascending motion in the Tropics and a descent flow over the polar regions helps shape the meridional structure of tropopause height (Thuburn and Craig, 2000; Birner, 2010; Haqq-Misra *et al.*, 2011; Zurita-Gotor and Vallis, 2013). In particular, Thuburn and Craig (2000) applied an anomalous zonal force in the stratosphere to modulate the residual circulation and found that a stronger stratospheric circulation tends to lift the tropical tropopause and suppress the polar tropopause. Birner (2010) found that, without the stratospheric circulation, the stratospheric radiative equilibrium solutions are characterized by a much reduced Equator-to-pole contrast in tropopause height (2–3 km), consistent with our calculations (Figure 4). Haqq-Misra *et al.* (2011) further confirmed this argument by showing that extratropical baroclinic eddies, a driver of the Brewer–Dobson circulation, are important in shaping the meridional structure of tropopause height. Here we briefly discuss the basic physics behind these arguments and show that our semianalytic model leads to similar conclusions, with the novel aspect being that we are able to put the equatorial tropopause into the context of a general theory of tropopause height with separate dependences on various factors (e.g., lapse rate, stratospheric heating) made explicit.

The tropical upward motion in the highly stratified stratosphere induces strong dynamical cooling Q_s that breaks the radiative balance we previously assumed. As a result, Equation 4 needs to be modified to become

$$\frac{\partial I}{\partial \tau} + Q_s = 0, \quad (13)$$

where $Q_s = \rho c_p \dot{Q} d\tau/dz$. Here \dot{Q} is the dynamical heating rate in K/s, ρ is atmospheric density, and $c_p = 1005 \text{ J}/(\text{kg K})$ is the heat capacity of air. If the vertical profile of Q_s is given, we can (see Appendix) obtain the stratospheric radiative–dynamical equilibrium temperature profile

$$T_{\text{rde}} = \left[\left(\frac{\tau + 1}{2\sigma} \right) \text{OLR} + \frac{Q_s - \overline{Q_s}}{2\sigma} \right]^{\frac{1}{4}}, \quad (14)$$

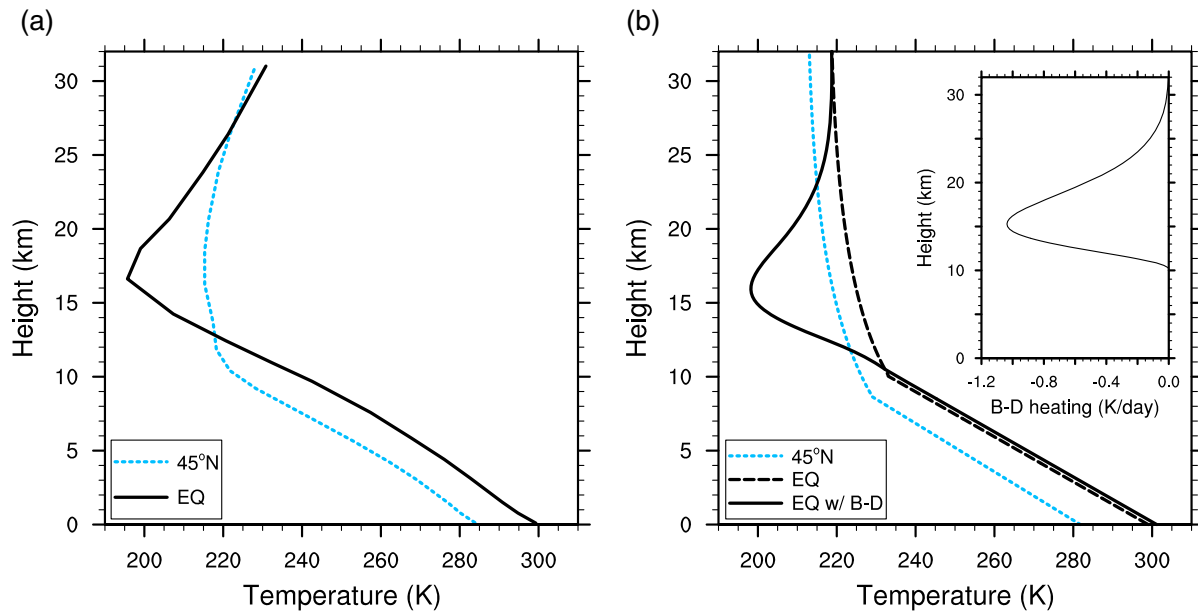


FIGURE 5 (a) Annual-mean zonal-mean temperature profiles at the Equator solid and 45°N (dotted) in NCEP2. (b) Same as panel (a) but derived from our simple model; the dashed and solid lines are for equatorial temperature profiles without and with a dynamical cooling representing that of the Brewer–Dobson circulation. The dynamical cooling profile is embedded in panel (b), and its peak value is 1 K/day, similar to that for the current climate [Colour figure can be viewed at wileyonlinelibrary.com]

where $\overline{Q_s(\tau)} = \int_0^\tau \int_0^{\tau'} Q_s(\tau'') d\tau'' d\tau'$. After replacing T_{re} with T_{rde} in Equation 10, again we can solve the system numerically by iterating over the different values of H_T until the surface boundary condition ($U = \sigma T_s^4$) is matched. (Details of how the numerical solutions are obtained are presented in the Appendix.) The numerical solution of H_T then gives the boundary between the lower region where the lapse rate is specified and the upper radiative–dynamical region. This may be the top of the deep convective region in the Tropics but the tropopause itself, as given by the usual WMO lapse-rate definition, may be much higher, as we now discuss.

An example calculation is shown in Figure 5b. We impose an equatorial dynamical cooling that peaks around 150 hPa and decreases sinusoidally with pressure upward and downward within 20–280 hPa; its vertical profile is embedded in Figure 5b. We choose a peak cooling magnitude of about 1 K/day, similar to that found in reanalysis products (Fueglistaler *et al.*, 2009; Birner, 2010). For other variables (i.e., OLR, Γ , τ_{ws} , and τ_{ds}), we use their observed values at the Equator that are used to produce Figure 4. For comparison, we also plot the modelled temperature profile at 45°N using the corresponding input values as observed, with no Brewer–Dobson cooling. The imposed dynamical cooling cools the lower stratosphere/upper troposphere substantially. It gives rise to an elevated tropopause layer (16 km based on the cold point) that is significantly cooler than the midlatitude tropopause, in agreement with observations (Figure 5a) and broadly consistent with Thuburn and Craig (2000). Note that

the cold-point tropopause here (~ 16 km), or similarly a thermal tropopause such as that given by the WMO definition, is above the location of H_T , which by definition is at the top of the deep convective region (~ 10.5 km). This suggests that a thermal (or WMO) tropopause is not in fact a particularly good demarcation between the dynamics of the troposphere and stratosphere, consistent with the notion that the thermal structure of the tropical tropopause is greatly influenced by the stratospheric circulation (Highwood and Hoskins, 1998; Fueglistaler *et al.*, 2009). In high latitudes, the downwelling-induced adiabatic warming due to the stratospheric circulation may shift the tropopause downward, but this effect is smaller than that due to upwelling in the Tropics (Birner, 2010; Haqq-Misra *et al.*, 2011).

In the absence of ozone heating, the model does not show as large a rise in temperature above the tropopause as is seen in the observations (Figure 5). We remedy this by adding an ozone-induced solar heating rate to Q_s in Equation 13, and sample results are shown in Figure 6. Here we imposed an additional heating rate that peaks around 55 km at a value of about 2 K/day (see the embedded profile in the figure). The resultant temperature profile agrees better with the observations, but experiments show that the ozone-induced heating rate has only a small effect on tropopause height and temperature, consistent with Thuburn and Craig (2000).

We now turn our attention to how the tropopause height and temperature change in a warmer climate. We focus on the role of water-vapour path, tropospheric lapse rate, and outgoing longwave radiation; we will find that they alone

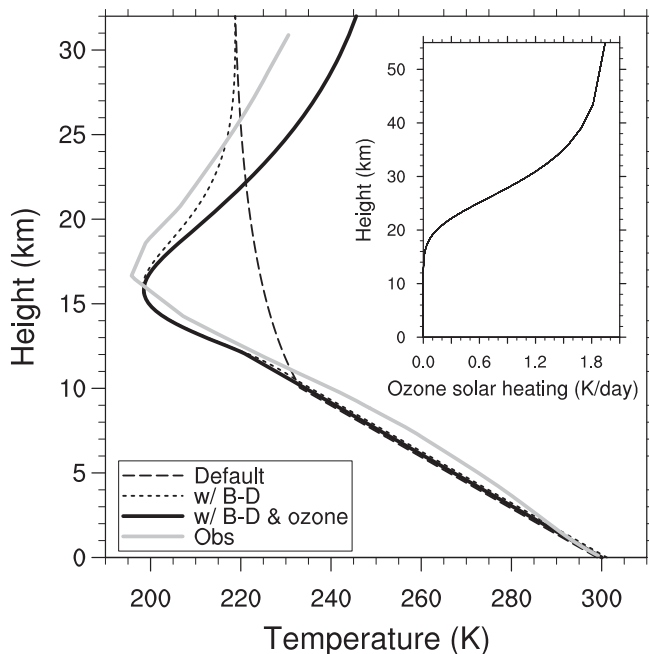


FIGURE 6 Temperature profiles at the Equator derived from the radiative–convective model (black). The dashed line is for the default radiative–convective model; the dotted line is with a dynamical cooling representing that of the Brewer–Dobson circulation; the solid line is with an ozone-induced solar heating in addition to the dynamical cooling. The ozone heating profile is embedded, and its peak value is about 2 K/day at 55 km. The annual-mean zonal-mean temperature profile at the Equator from NCEP2 (grey) is shown for comparison

capture the future changes of tropopause height in both the multimodel mean and the intermodel spread.

6 | TROPOPAUSE HEIGHT CHANGES IN A WARMER CLIMATE

6.1 | CMIP5 analyses

In the next two sections, we will apply our simple tropopause model to understand better future changes of tropopause height and temperature in the warmer climates projected by the CMIP5 models. One of the most robust features of atmospheric large-scale circulation response to global warming is the increase of tropopause height (Santer *et al.*, 2003; Lorenz and DeWeaver, 2007; Lu *et al.*, 2008; Vallis *et al.*, 2015). Consistent with these studies, we find a robust upward shift of the tropopause at all latitudes across all models (Figure 7a). In the multimodel mean, the tropopause shifts upward with a rate of 0.6–0.8 km per century depending on latitude. Although the increase is robust, there is a large intermodel spread in its magnitude, with the spread being particularly large in the Tropics.

To understand these features better, we investigate the connection between changes in tropopause height and changes in water-vapour path, tropospheric lapse rate, and outgoing

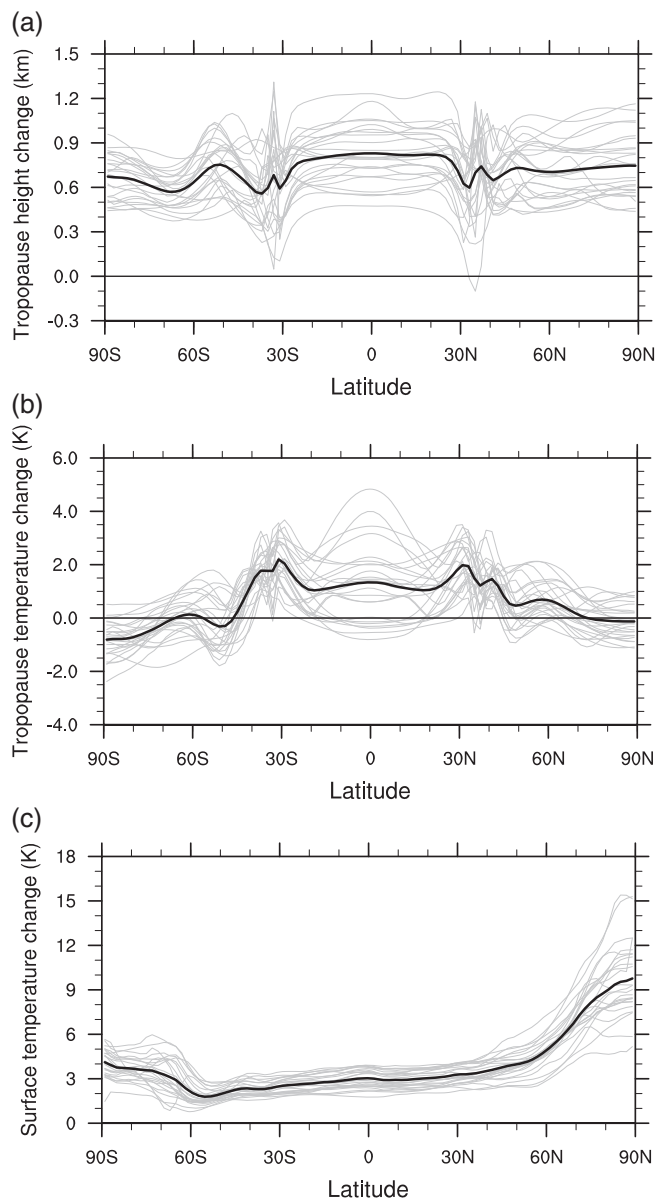


FIGURE 7 Changes over a century in annual-mean zonal-mean (a) tropopause height, (b) tropopause temperature, and (c) surface temperature for the 1% scenario as a function of latitude. Grey lines are for each individual CMIP5 model, and black lines highlight the multimodel averages

longwave radiation, the three main controlling factors suggested by our tropopause model. On average, water-vapour path increases by 12 mm over a century at the Equator (Figure 8a); its relative change is about 30% globally and peaks over the high latitudes (40–50%). The intermodel spread in the water-vapour path changes is positively and significantly correlated with the tropopause height changes for almost all latitudes ($p < 0.01$), except for the high latitudes of the Southern Hemisphere, and the highest correlation (>0.8) is found over the Tropics and the Arctic (Figure 9a).

The tropospheric lapse rate decreases in the Tropics, following the decrease in saturated adiabatic lapse rate in

a warming climate (Figure 8b). However, the lapse rate increases over the polar regions, particularly over the Arctic, because polar amplification is mostly confined to the thermally stable lower troposphere. The intermodel spread of the tropospheric lapse rate changes is negatively correlated with the tropopause height changes over the broad Tropics and subtropics within 50°S–50°N, and the peak correlation exceeds 0.8 (Figure 9b).

The outgoing longwave radiation change shows a more complicated meridional structure, and the intermodel spread is larger than the multimodel mean over latitude (Figure 8c). This structure reflects the fact that outgoing longwave radiation is affected by a variety of factors involving both external forcing (CO_2) and internal climate feedbacks (water vapour, clouds), as well as changes in meridional heat transport. The magnitude of the resultant outgoing longwave radiation change is quite small. The intermodel spread of the outgoing longwave radiation changes is only weakly correlated with the tropopause height changes over the Northern subtropics and high latitudes and some of the Southern subtropics, and most of the correlations do not pass the 1% significance level (Figure 9c). Although the change in net outgoing longwave radiation is positive, the change in top-of-atmosphere net radiation, incoming net shortwave minus outgoing longwave, is actually positive because the incoming shortwave increases, at least partly because of a reduction in ice cover.

6.2 | Causes of tropopause height changes

We now employ our model to interpret the tropopause height changes seen in the CMIP5 models quantitatively. We start from the background meridional structure of tropopause height calculated according to NCEP2 (i.e., the thick grey line in Figure 4). We perturb the NCEP2 input variables (i.e., water-vapour path, tropospheric lapse rate, and outgoing longwave radiation) with the projected changes in each CMIP5 model, and estimate the resultant changes in the tropopause height. We repeat the procedure for each variable, with the rest being unchanged, to isolate their individual contribution.

For the impact of CO_2 , we use a slightly different approach, since the radiative forcing of CO_2 is relatively better constrained in climate models. The 1%/year increase of CO_2 will lead to a factor of 2.7 CO_2 concentration increase after one century, corresponding to a radiative forcing of $+5.3 \text{ W/m}^2$, scaling from $+3.7 \text{ W/m}^2$ per CO_2 doubling [$3.7 \times \log(2.7)/\log(2) = 5.3$]. Based on our model estimate, a reduction of outgoing longwave radiation by 5.3 W/m^2 without changes in temperature profiles would require an increase of dry-air surface optical depth τ_{ds} in Equation 11 by 0.11. Therefore, the impact of the CO_2 increase over a century can be estimated by increasing τ_{ds} by 0.11 uniformly for each latitude and calculating the changes in tropopause height.

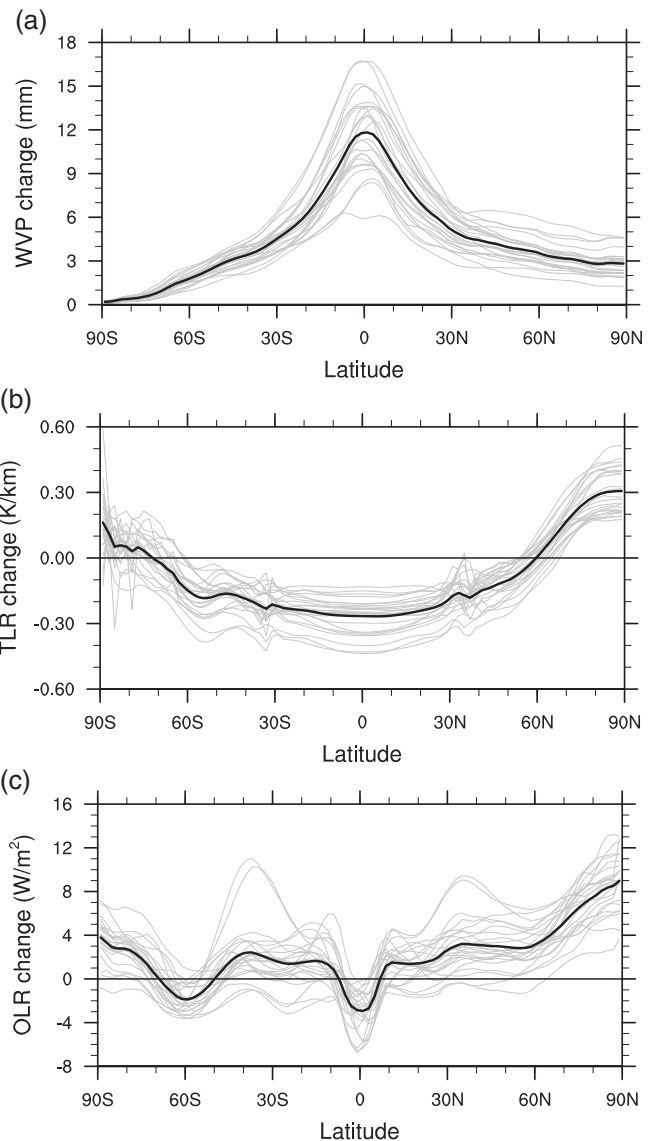


FIGURE 8 Changes in (a) water-vapour path (WVP), (b) tropospheric lapse rate (TLR), and (c) outgoing longwave radiation (OLR) over a century for the 1% scenario, as a function of latitude. Grey lines are for each individual CMIP5 model, and black lines highlight the multimodel mean

Unlike the aforementioned three factors, we have estimated the effect of CO_2 only once, because its uncertainty and hence variation among the models is relatively small.

For all the above effects we proceed numerically, since our numerical solutions are more general than the analytic ones, but the changes may largely be interpreted by an analysis of Equation 12. We conduct the calculations separately for each latitude and for each CMIP5 model, and the multimodel-mean results are summarized in Table 1. With all four factors considered, the simple model predicts the tropical-mean tropopause height change seen in the CMIP5 models (0.78 km versus 0.80 km) with an error of less than 3%. Among them, the increase of water-vapour path acts as the dominant factor (about 48%), followed by the reduction of

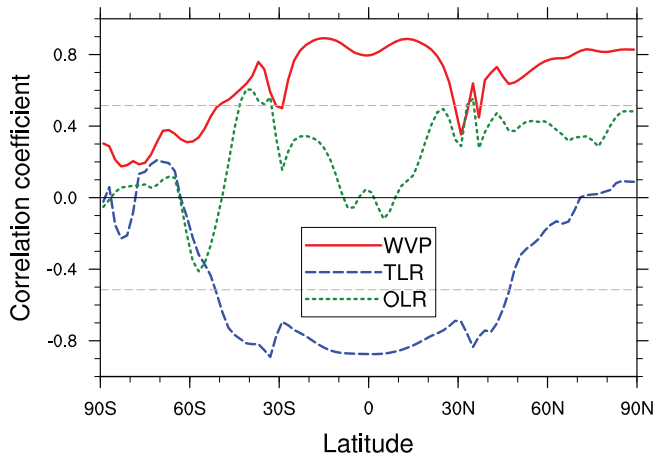


FIGURE 9 Linear correlation coefficients between the tropopause height changes and the changes in water-vapour path (WVP, solid), tropospheric lapse rate (TLR, dashed), or outgoing longwave radiation (OLR, dotted) among the CMIP5 models, as a function of latitude. The two light dashed lines highlight the significance level ($p < 0.01$) of the Pearson correlation [Colour figure can be viewed at wileyonlinelibrary.com]

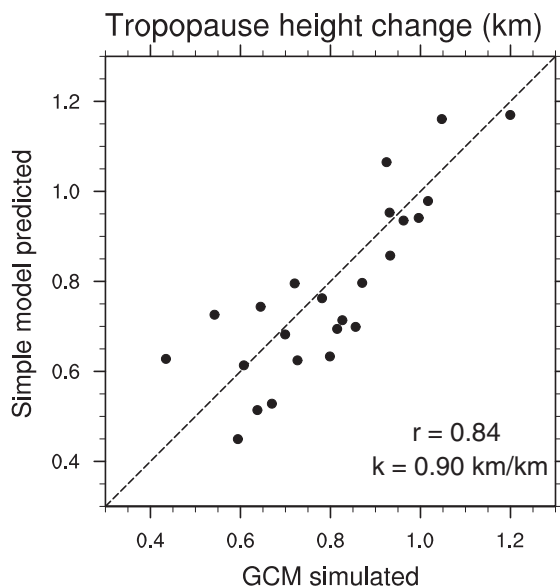


FIGURE 10 Intermodel scatter diagram for model-predicted versus GCM-simulated tropopause height changes for the 1% scenario. The correlation (r) and regression (k) coefficients are shown in the bottom-right corner of the diagram

tropospheric lapse rate (44%). Although change in CO_2 is the only external forcing, its direct contribution to the tropopause height increase is quite small (4%). The effect of changes in outgoing longwave radiation is even smaller, less than 1%. These percentages should not be taken as exact, but we quote them because they are indicative of the magnitude of the effects. Our results confirm the finding by Vallis *et al.* (2015) that the increase of water-vapour path and the reduction of

tropospheric lapse rate are two key processes contributing to the rise of the tropopause under greenhouse warming.

We further applied the simple model to study the spread of tropopause height changes projected for the GCMs. The model captures the spread of the tropopause height changes among the CMIP5 models quite accurately (Figure 10), and the intermodel correlation coefficient is as high as $r = 0.84$. The scattered dots almost fall on to a one-to-one line—the simple model predicts the tropopause height change for each individual CMIP5 model surprisingly well. The skill of the simple model is less in the midlatitudes and breaks down in high latitudes (not shown), consistent with the fact that high correlations are mainly found in the Tropics (Figure 9). The lower skill in mid and high latitudes may be partly due to the lack of “tightness” of the radiative constraint, meaning that small changes in the tropopause height do not necessarily lead to large changes in outgoing radiation (Zurita-Gotor and Vallis, 2013). At high latitudes, the presence of a low-level inversion also makes the simple model less appropriate. When averaged over the whole globe, the simple model underestimates the tropopause height changes (Table 1) and the intermodel correlation becomes slightly weaker ($r = 0.82$). As we noted in section 3, another potential weakness of the model is that it is grey in the infrared and we look at this effect in section 7.4.

7 | TROPOPAUSE TEMPERATURE CHANGES

We now look at possible changes in tropopause temperature under global warming. Among other things, the tropical tropopause temperature is important in determining the stratospheric water-vapour amount (Mote *et al.*, 1996) and the intensity of tropical cyclones (Emanuel *et al.*, 2013; Wang *et al.*, 2014). Now, the emission temperature at any particular latitude will not change significantly unless there are large changes in meridional heat transport, which seems unlikely in the foreseeable future under most warming scenarios. Under these circumstances, the tropopause temperature, which is tied to the emission temperature, should stay roughly constant under greenhouse warming. The constant-temperature result is exact in a grey model with a troposphere in radiative–convective equilibrium) and an optically thin stratosphere in radiative equilibrium (Vallis *et al.*, 2015).

A seemingly related hypothesis is that tropical anvil clouds occur at a nearly constant temperature in a warming climate (Hartmann and Larson, 2002; Kuang and Hartmann, 2007; Li *et al.*, 2012). This idea, often termed the Fixed Anvil Temperature (FAT) hypothesis, has also been applied to the extratropics (Thompson *et al.*, 2017), where the clear-sky diabatic mass flux is presumed to vanish at roughly a fixed water-vapour concentration, as in the Tropics. Some deep convective clouds

TABLE 1 CMIP5-informed simple model estimates of tropopause height changes in a warming climate. Tropical-mean and global-mean results are shown separately. Attribution analysis is conducted for each individual factor, including water-vapour path (WVP), tropospheric lapse rate (TLR), outgoing longwave radiation (OLR), and carbon dioxide (CO₂). “All” refers to the case incorporating all the four factors. “CMIP5” refers to the results computed from the outputs of the 24 CMIP5 model. Both the multimodel mean and intermodel spread, measured by standard deviation, are shown. See the main text for details of the calculations

	WVP	TLR	OLR	CO ₂	All	CMIP5
Tropical mean (km)	0.39±0.08	0.35±0.11	0.00±0.01	0.03	0.78±0.20	0.80±0.18
Global mean (km)	0.34±0.07	0.26±0.10	0.01±0.01	0.04	0.65±0.17	0.74±0.16

ascend up to the tropopause and some observational products even assign the cloud-top temperature based on the tropopause temperature (Marchand *et al.*, 2010). However, although they appear related, the constant-tropopause temperature hypothesis and the FAT hypothesis do arise from rather different arguments and there is no obvious guarantee that the two (tropopause temperature and anvil cloud-top temperature) should always covary with each other, especially if the tropopause and cloud top are well separated, as they sometimes are in the Tropics.

Changes in tropopause temperature (using the WMO definition) under global warming at each latitude in the CMIP5 models are shown in Figure 7b. We see that the tropopause temperature in the extratropics and the polar regions (i.e., poleward of 45°N and 45°S) indeed varies little compared with the surface warming, consistent with the radiative and thermodynamic constraints discussed above. However, some tropopause warming is found at the tropical tropopause within 30°S–30°N, although there is a large intermodel spread, and the warming is only half that at the surface (Figure 7c). A similar warming trend at the tropical tropopause has been identified in observations and modelled future warming scenarios (Austin and Reichler, 2008; Kim *et al.*, 2013; Lin *et al.*, 2017), although a near-constant tropical tropopause temperature was apparently found with a cloud-resolving model by Seeley *et al.* (2019). These results do not speak directly to the FAT hypothesis, since the tropical tropopause may be well above the anvil cloud top and the changes in the two are not necessarily coupled.

To understand better the causes of the increase in tropopause temperature, we impose the changes in CO₂, water-vapour path, tropospheric lapse rate, and outgoing longwave radiation under the 1% scenario from each model (as was done in section 6.2). Note that, although the model is grey in the infrared (a restriction we relax below), the stratosphere has a finite optical depth because of the presence of carbon dioxide and is not isothermal, so that the fixed tropopause temperature result is not exact. In fact, as the water-vapour path increases or the tropospheric lapse rate decreases, the tropopause height will increase and thus the tropopause temperature will actually decrease slightly, if there is an unchanged radiative equilibrium temperature profile in the stratosphere, given that $T_{re} = [(\tau + 1)OLR/(2\sigma)]^{1/4}$. However, this is not the only

effect. As the CO₂ concentration increases, its scale height is sufficiently large that the stratospheric optical thickness increases and thus T_{re} increases, and this leads to an increase in tropopause temperature. Finally, an outgoing longwave radiation increase (decrease) will tend to increase (decrease) the tropopause temperature by increasing (decreasing) T_{re} . (A rough estimate of the magnitude of the tropopause warming, ΔT , due only to changes in outgoing longwave radiation of ΔOLR is obtained by using Equations 8 and 9 with $\tau = 0$. For small ΔT , we have $4\Delta T_T/T_T = \Delta OLR/OLR$, where $T_T = T_{re}$ is the tropopause temperature, which gives $\Delta T \approx 0.5^\circ\text{C}$.)

After taking into account all the above factors, the grey model predicts an almost unchanged tropical tropopause temperature (0.03 °C per century), in contrast to the more substantial tropopause warming found in the CMIP5 models (about 1.3 °C per century on average, shown in Figure 7). To understand this result better, we will increase the complexity of our radiative model, but in the most minimal way, as follows.

7.1 | An infrared window

The real atmosphere is not grey to infrared radiation and atmospheric opacity varies with wavelength, as was known to Arrhenius (1896) and Simpson (1928). To capture the essence of the nongreyness, let us construct a model with two bands in the infrared, a window band (8–13 μm; denoted with the superscript “win”) and the nonwindow infrared band (marked with the superscript “lw”), which contains all infrared absorption except that within the window band; the nonwindow band is where most of the infrared absorption occurs. (When we refer to the “two-band” model and the “grey” model, we mean two bands in the infrared and grey in the infrared, respectively, without reference to solar radiation.) The modified radiative transfer equations become

$$\frac{\partial D^{lw}}{\partial \tau^{lw}} = \beta B - D^{lw}, \quad \frac{\partial U^{lw}}{\partial \tau^{lw}} = U^{lw} - \beta B, \quad (15)$$

and

$$\frac{\partial D^{win}}{\partial \tau^{win}} = (1 - \beta)B - D^{win}, \quad \frac{\partial U^{win}}{\partial \tau^{win}} = U^{win} - (1 - \beta)B. \quad (16)$$

Here, β and $1 - \beta$ represent the nonwindow fraction and window fraction of the emitted infrared radiation, respectively. This is similar to the model in Weaver and Ramanathan (1995), but here we assume a small but finite optical depth for the window region, as in Geen *et al.* (2016) and Vallis *et al.* (2018), and following those authors we choose $\beta = .63$. The nonwindow optical depth has the same expression as the grey-atmosphere one,

$$\tau^{\text{lw}} = \tau_{\text{ws}}^{\text{lw}} \exp(-z/H_a) + \tau_{\text{ds}}^{\text{lw}} \exp(-z/H_s). \quad (17)$$

However, the values of surface optical depth must be increased to account for the fact that only a portion of the infrared radiation goes through this band. For the window region, the main absorbers are ozone (which we do not treat here) and water vapour (e.g., Andrews, 2010, figure 3.14), and thus we take the window optical depth to vary as

$$\tau^{\text{win}} = \tau_{\text{ws}}^{\text{win}} \exp(-z/H_a). \quad (18)$$

The surface optical depth in the window region is quite small compared with that in the nonwindow region.

As in the grey-atmosphere configuration, we assume that the stratosphere is in radiative equilibrium, which now requires

$$\frac{\partial(U^{\text{lw}} + U^{\text{win}} - D^{\text{lw}} - D^{\text{win}})}{\partial z} = 0. \quad (19)$$

Since the stratospheric optical depth is extremely small in the window band, U^{win} and D^{win} are nearly constant with height. As a result, the primary balance in Equation 19 is between $\partial U^{\text{lw}}/\partial z$ and $\partial D^{\text{lw}}/\partial z$. In other words, the nonwindow band is in near-radiative equilibrium in the stratosphere, namely,

$$\frac{\partial(U^{\text{lw}} - D^{\text{lw}})}{\partial z} \approx 0. \quad (20)$$

The system is closed by the top-of-atmosphere boundary conditions: $D^{\text{lw}} = 0$, $D^{\text{win}} = 0$, $U^{\text{lw}} = \text{OLR}^{\text{lw}}$, and $U^{\text{win}} = \text{OLR}^{\text{win}}$, where $\text{OLR}^{\text{lw}} + \text{OLR}^{\text{win}} = \text{OLR}$. In addition, we have the surface boundary conditions: $U^{\text{lw}} = \beta \sigma T_s^4$ and $U^{\text{win}} = (1 - \beta) \sigma T_s^4$, where T_s is surface temperature.

7.2 | Window versus nonwindow band: Idealized calculations

There are similarities between the nonwindow band and the grey-atmosphere model in terms of formulation, specifically in the equivalence of Equations 20 and 4. In the stratosphere, where τ^{win} is negligible, the radiative equilibrium temperature in the two-band model is given by

$$T_{\text{re}} = \left[\left(\frac{\tau^{\text{lw}} + 1}{2\sigma} \right) \text{OLR}^{\text{lw}} \right]^{1/4}. \quad (21)$$

Of course it is OLR that is a boundary condition in the model, not OLR^{lw} , but Equation 21 will be a useful relation, as discussed below. Equation 21 is very similar to Equation 9, the equivalent expression in the grey model.

In the grey model, an increase of τ in the troposphere leads to very little change in tropopause temperature, because the tropopause is simply extending into a nearly isothermal lower stratosphere. However, in a windowed model the response depends on whether the increase in optical path occurs in the window or nonwindow region, as we now illustrate with some idealized calculations (Figure 11). For the purpose of schematic illustration, we assume that water vapour is the only infrared absorber in the atmosphere for both the grey model and the windowed model ($\tau_{\text{ds}} = 0$, $\tau_{\text{ds}}^{\text{lw}} = 0$). We set $\text{OLR} = 260 \text{ W/m}^2$ and tropospheric lapse rate $\Gamma = 6 \text{ K/km}$. We set the surface optical depth $\tau_{\text{ws}} = 4$ for the grey model, $\tau_{\text{ws}}^{\text{lw}} = 8$, and $\tau_{\text{ws}}^{\text{win}} = 1$ for the two-band model. We assume that the surface optical depth increases by 50% under global warming and investigate the tropopause changes in three cases: (i) the grey model, and, for the two-band model, (ii) an increase in optical depth in the nonwindow region only, and (iii) an increase in the window region only.

In case (i), as noted, the tropopause temperature stays virtually constant in the grey model (Figure 11a). In case (ii), we incorporate the water-vapour path increase solely as an increase in $\tau_{\text{ws}}^{\text{lw}}$, while keeping the optical depth in the window band unchanged. In response to the $\tau_{\text{ws}}^{\text{lw}}$ increase, the surface temperature increases, the troposphere warms, OLR^{win} increases (because the increased infrared radiation emitted from the ground passes upwards virtually unobstructed), and therefore OLR^{lw} must decrease to keep total outgoing long-wave radiation the same. For a 50% increase of $\tau_{\text{ws}}^{\text{lw}}$, we find that the equilibrium $\Delta \text{OLR}^{\text{lw}} = -\text{OLR}^{\text{win}} = -4.8 \text{ W/m}^2$. From Equation 21, the reduction of OLR^{lw} implies that the stratospheric temperature falls (note that τ^{lw} is small in the stratosphere when water vapour is the only infrared absorber). A warmer troposphere and a cooler stratosphere suggest that they have to meet at a higher level (i.e., there is an increase of tropopause height) and at a colder temperature (i.e., a decrease of tropopause temperature), and the results of the calculation are shown with a red line in Figure 11b.

In case (iii), we incorporate the water-vapour path increase as an increase in $\tau_{\text{ws}}^{\text{win}}$, keeping the optical depth in the nonwindow band unchanged. In response to the $\tau_{\text{ws}}^{\text{win}}$ increase, the surface temperature increases, the troposphere warms, and OLR^{lw} increases (because the warmer troposphere emits greater infrared radiation and the nonwindow optical depth is unchanged). The increase of OLR^{lw} implies that the stratospheric temperature increases. A warmer troposphere and a warmer stratosphere suggest that they have to meet at a warmer tropopause. The increase in tropopause temperature can also be revealed by a simple argument for the

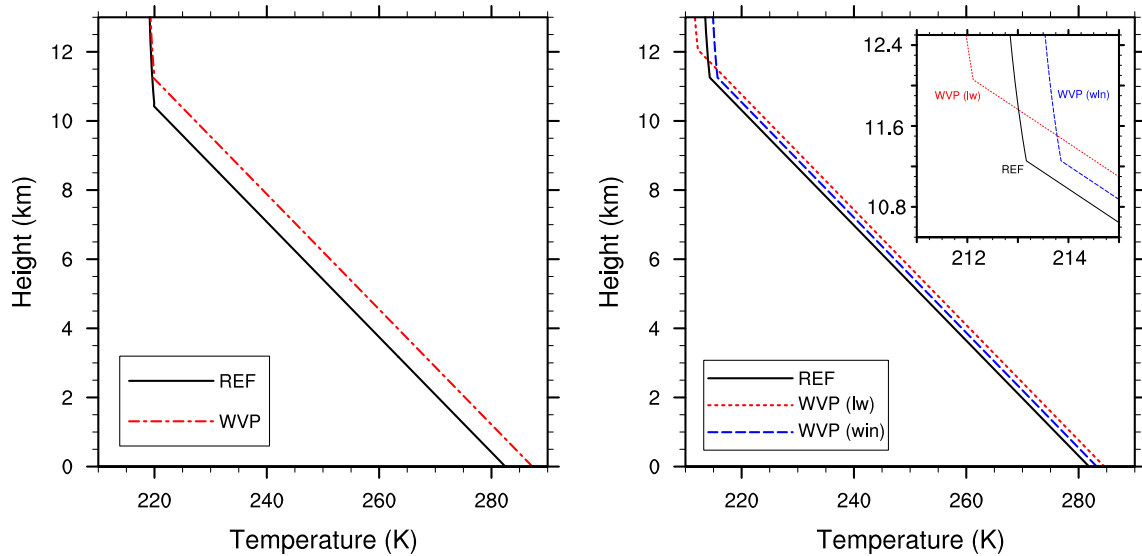


FIGURE 11 Temperature profile response to water-vapour path increase in (a) the grey model and (b) the two-band model. In the reference case (REF), we set $OLR = 260 \text{ W/m}^2$, tropospheric lapse rate $\Gamma = 6 \text{ K/km}$, and surface optical depth $\tau_{ws} = 4$ for the grey model, $\tau_{ws}^{lw} = 8$ and $\tau_{ws}^{win} = 1$ for the two-band model. For each WVP case, we assume that the surface optical depth increases by 50% [Colour figure can be viewed at wileyonlinelibrary.com]

window band. The outgoing longwave radiation in the window band nearly all comes from the surface, and is equal to $(1 - \beta)Tr\sigma T_s^4$ where, Tr is the transmissivity of the atmosphere. Now T_s increases as the water-vapour path increases, but Tr decreases because there is more atmospheric absorption. If the Tr decrease is sufficiently large, there will be *less* radiation to space from the ground in the window region. As a result, the increase of OLR^{lw} and the reduction of OLR^{win} together lead to an unchanged OLR. A calculation with the two-band model illustrates this effect more quantitatively—see the blue line in Figure 11b. In response to a 50% increase in τ_{ws}^{win} , the surface temperature and tropospheric temperature both increase, but the tropopause height does not change very much (Figure 11b). Then, given the unchanged optical depth profile in the non-window band, there is an increase in OLR^{lw} ($+3.2 \text{ W/m}^2$ for this case), compensating for the decrease in OLR^{win} and keeping the total OLR the same.

To summarize, the effect of an increase of water-vapour path on tropopause temperature is sensitive to the presence of an infrared window, an effect that to our knowledge has not previously been investigated. If the window is closed by an increase in water-vapour content, then the tropopause temperature must increase to keep the total outgoing longwave radiation constant. In the following section, we see to what extent it is important in CMIP5 models, noting that more realistic (multiband) calculations are needed to quantify the effect better.

7.3 | Window versus nonwindow band: CMIP5 analyses

In reality, the optical depths in both the window and non-window bands may increase, potentially leading to increases in both tropopause height and temperature, as is seen in the CMIP5 models. To illustrate this, we set the model parameters to more realistic values and, in particular, we now add back the contribution of carbon dioxide to the nonwindow optical depth. We set $\tau_{ds}^{lw} = 2.6$ and $\tau_{ws}^{lw} = \alpha^{lw}WVP$, where $\alpha^{lw} = 0.26 \text{ mm}^{-1}$. We set $\tau_{ws}^{win} = \alpha^{win}WVP$, where $\alpha^{win} = 0.0125 \text{ mm}^{-1}$. In the Tropics, the water-vapour path is in the range 20–40 mm (Figure 3a), and this can be translated into a τ_{ws}^{win} range of about 0.25–0.5. It corresponds to a range of absorption percentage of about 20–40%. Note that the infrared absorption and emission in the window band are more important in the Tropics than elsewhere (e.g., Huang *et al.*, 2014), because of the larger amount of water vapour. The resultant mean climate generally resembles that from the grey-atmosphere model, and has a global mean surface temperature of 15°C .

We then use the model parameters given above and impose the changes in input variables (WVP, TLR, OLR, and CO_2) from the CMIP5 models on the NCEP2 basic state. For the first three input variables, they are first averaged across the various GCMs and across the latitudinal bands in the Tropics (30°S – 30°N), and then applied to the two-band model. For CO_2 , an equivalent τ_{ds}^{lw} increase of 0.43 is imposed, which would roughly give rise to a radiative forcing of an increase of CO_2 by a factor of 2.7, which is about 100 years of 1%/year increase). We perform experiments with the water-vapour

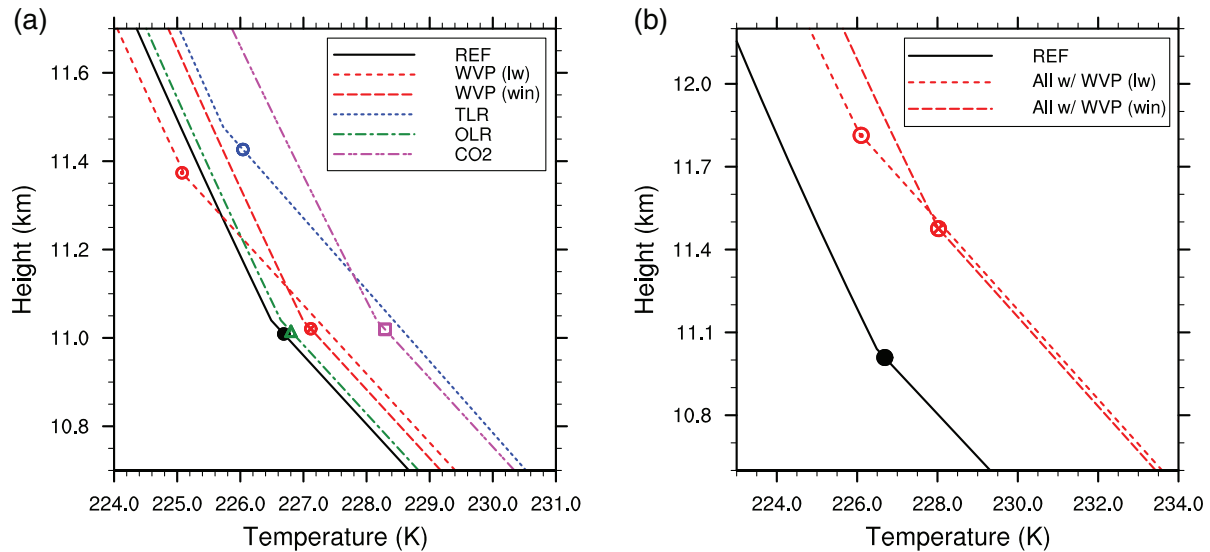


FIGURE 12 (a) Temperature profiles and point of tropical tropopause produced by the two-band tropopause model. “REF” refers to the reference state using tropical mean (30°S–30°N) NCEP2-informed input variables. “WVP (lw)” and “WVP (win)” refer to the cases where CMIP5 water-vapour path changes are incorporated as the optical depth increase in the nonwindow and window regions, respectively, while other input variables remain unchanged. “TLR”, “OLR”, and “CO2” refer to the cases with the CMIP5 changes in tropospheric lapse rate, outgoing longwave radiation, and carbon dioxide, respectively, alone. (b) Similar to panel (a), but for the cases with all four effects (WVP, TLR, OLR, and CO2) with the two distinctive treatments of WVP increase. For all the calculations, we first apply the tropical-mean multimodel-mean changes in input variables and then identify the tropopause (markers), here defined as in Equation 10, as the top of the region of imposed stratification [Colour figure can be viewed at wileyonlinelibrary.com]

optical path increased only in the nonwindow region, only in the window region, and in both.

The changes in tropopause height and temperature found in this more realistic configuration have the same characteristics as those found in the idealized calculations. In the case with τ_{ws}^{lw} alone increasing, the water-vapour path increase alone would lead to a decrease of tropical tropopause temperature by -1.6°C per century (Figure 12a). In the case with τ_{ws}^{win} alone increasing, the same water-vapour path increase would result in an increase of tropopause temperature by $+0.4^{\circ}\text{C}$ per century. After accounting for all four factors (CO₂, WVP, TLR, and OLR), the model predicts a tropical tropopause temperature change of -0.6°C for the nonwindow case and $+1.4^{\circ}\text{C}$ per century for the window case (Figure 12b). The calculation in which the increase in optical depth is split across window and nonwindow regions (not shown) lies between these two cases.

The results from the case in which the optical path increases in the window region agree quite well with the CMIP5 model projections (about 1.3°C per century). However, the spread in tropopause temperature changes across the individual CMIP5 models is not well captured by the two-band model (not shown). The real atmosphere has the contribution from both effects, but the effect associated with the window case most likely dominates, in particular over the Tropics (Huang *et al.*, 2014), because the infrared absorption in the nonwindow band is nearly saturated and the overlap

of absorption between CO₂ and water vapour is particularly large.

7.4 | Tropopause height changes in the windowed model

We see in Figure 12 that if the increase in optical depth is in the window region then the tropopause height increase is smaller than if the optical depth increase is in the nonwindow region, which in turn is similar to the grey-model predictions. To explore this further, we repeat the calculations described in Section 7 with the two-band model, and results analogous to those of Figure 10 are shown in Figure 13. If the optical path increase is applied solely to the nonwindow region, as in Figure 13a, then the results are very similar to those of the grey model. If the optical path increase is applied in the window region, then the tropopause height increase is systematically smaller. This result is expected, because changes in the optical path in the window region have only a small direct effect on changes in tropopause height, and the increase in height is due mostly to changes in lapse rate; the height change is therefore smaller than when the optical path increases in the nonwindow region. There is, nevertheless, still a very good correlation between the simple model and the GCM results in all cases. In reality, an increase in water-vapour content will affect both the window and nonwindow parts of the spectrum, in

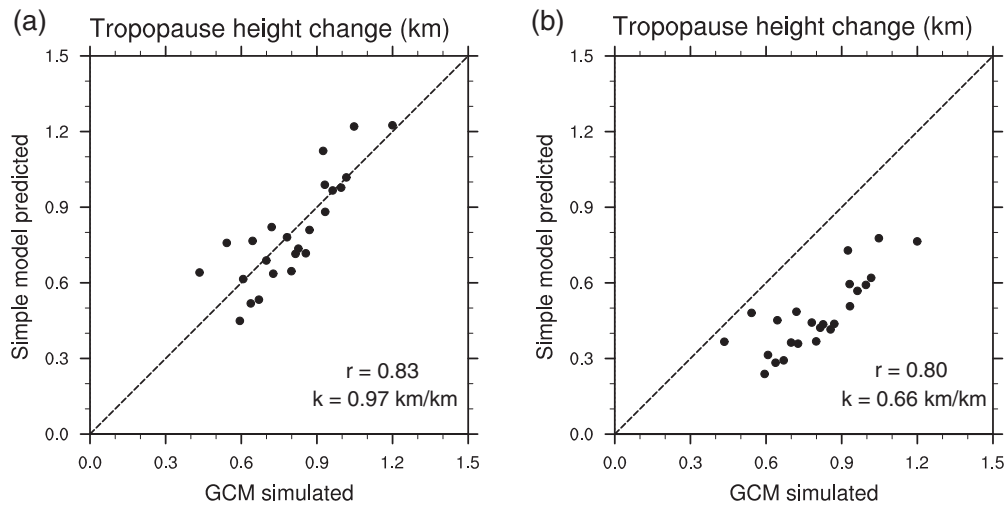


FIGURE 13 As for Figure 10, showing scatter plots of model-predicted versus GCM simulations of tropopause height, but now using the two-band model. (a) Optical depth increase in the nonwindowed region only. (b) Optical depth increase in the windowed region only

different proportions depending on water-vapour content and cloudiness, leading to an increase in both tropopause height and temperature. A quantitative treatment of all these effects would require not only a full multiband radiation model but also a good model of clouds, which is beyond our scope.

It is evident that the grey model captures the future increases in tropopause height, with some quantitative changes then arising from the nongreyness of the atmosphere. However, changes in tropopause temperature, although small compared with changes in surface temperature, require a windowed radiative model to explain them. (The grey model does explain the lowest-order result that tropopause temperature changes are small compared with surface temperature changes.) There are of course other potential mechanisms that might affect the tropopause height and temperature that occur in GCMs but are not considered in our study, such as changes in dynamical cooling induced by the stratospheric circulation because of changes in the Brewer–Dobson circulation or ozone heating.

8 | SUMMARY AND CONCLUSIONS

In this study we have used a relatively simple column model to understand the meridional structure and possible future changes of height and temperature of the tropopause associated with global warming. The model assumes a troposphere with a given lapse rate that connects continuously to a stratosphere in which the lapse rate is determined by either pure radiative balance or a radiative–dynamical balance. If we assume that the tropospheric lapse rate is determined by convection, then the model is essentially a radiative–convective model. The model explicitly exposes the dependence of tropopause height on the optical depth, tropospheric lapse

rate, and outgoing longwave radiation of the atmosphere. Thus, a greater optical depth or a smaller tropospheric lapse rate will elevate the tropopause, whereas the tropopause height is relatively insensitive to outgoing longwave radiation changes, as may be inferred from the approximate analytic solution in Equation 12.

When applied to the present climate, the model, even when configured with a stratosphere in radiative equilibrium, is able to reproduce the meridional shape of the tropopause height—one that is higher in the Tropics and lower in the polar regions, with a fairly sharp transition in the extratropics, as in Figure 4. The higher tropopause in the Tropics here results from the greater water-vapour path, but its impact is largely compensated by that of the larger tropical tropospheric lapse rate, which reduces tropopause height. As a result, the Equator-to-pole contrast in tropopause height predicted by the model is too small compared with the observations. If we incorporate a dynamical cooling profile to represent the impact of the stratospheric circulation, then the tropical tropopause is elevated and cooled, making it closer to what is observed, broadly consistent with the results of Thuburn and Craig (2000), Birner (2010), and Haqq-Misra *et al.* (2011). In this case, the tropical tropopause, as defined by a lapse-rate criterion, is well above the boundary between a convective region (with a given lapse rate) and a region where the lapse rate is determined by a balance between radiation and slow dynamics. A thermal (or WMO) tropopause is then not a particularly good demarcation between the dynamics of the troposphere and stratosphere.

The model may be used to disentangle the multiple factors affecting the change in tropopause height and temperature associated with global warming. An increase in tropopause height is one of the most robust consequences of such warming, predicted by nearly all CMIP5 models in nearly all

warming scenarios. In the 1% scenario (with CO₂ increasing by 1% per year) the annual-mean zonal-mean tropopause height increases, on average, by about 0.7 km within a century for all latitudes from the Equator to the poles. The main causes of the increase in height are the increase in optical depth (mainly associated with an increased water-vapour content) and decrease in lapse rate. These factors vary from model to model, giving rise to a large spread of the increase among the models. In lower latitudes (50°S–50°N), the intermodel spread is highly correlated with, and most likely due to, the differences in model-predicted changes in both water-vapour path and tropospheric lapse rate, while in high latitudes significant correlations are only found with the water-vapour path changes in the Northern Hemisphere.

Globally averaged, the grey model predicts the magnitude of tropical-mean tropopause height increase for each individual CMIP5 model quite well, after incorporating the effects of CO₂, water-vapour path, tropospheric lapse rate, and outgoing longwave radiation. (The intermodel correlation between the simple-model-predicted and GCM-simulated tropopause height changes is above 0.8, and the regression coefficient is close to one.) Among the four controlling factors, the contributions of changes in water-vapour path and lapse rate dominate, with the direct effects of changes in CO₂ and outgoing longwave radiation lagging far behind. Even though CO₂ is the only external forcing, its direct contribution to the tropopause height increase is small. The presence of an infrared window will make the water-vapour path effect a little less important, but still comparable to the lapse rate effect.

The tropopause temperature, as well as height, is found to increase in CMIP models with global warming, especially in low latitudes, although the average increase is much less than the surface temperature increase. Now, if the radiative transfer is grey in the infrared and if the stratosphere is in radiative equilibrium with a small optical depth, then the tropopause temperature will stay the same with global warming. That is, the “fixed tropopause temperature” hypothesis is exact in these circumstances. The small increase in tropopause temperature in more complex models and observations may, however, be explained by the presence of an infrared window, if an increase in optical depth occurs in the window region. In this circumstance, the outgoing longwave radiation in the window region decreases and must be compensated by an increase in outgoing longwave radiation from the nonwindow region, entailing an increase in tropopause temperature. The fact that temperature increases are greater at low latitudes, where water-vapour effects are strongest, is consistent with this hypothesis. In this article, we do not discuss the issue of whether and how changes in tropopause temperature are related to, or even violate, the fixed-anvil-temperature hypothesis.

The model we have presented and used has a number of limitations, and in particular it has limited skill in high latitudes. This is likely because a vertically uniform tropospheric lapse rate is not a good assumption in the presence of an inversion layer in the lower troposphere. (The model could be extended to have a nonuniform lapse rate, but then becomes a little arbitrary.) The model also makes a number of other assumptions and is (deliberately) not complete. For example, the lapse rate and water-vapour path are specified and not part of the model solution, nor are they parametrized in terms of surface temperature. Nor, by its very nature, does the column model treat meridional heat transfer, although the effects of that are in part captured by the use of observed outgoing longwave radiation. Thus, although the simple model enables an attribution to be made of why and how the various CMIP models differ in their responses, it does not explain the ultimate reasons for differences. Finally, in this article we have not investigated how future changes in the stratosphere (e.g., changes in the Brewer–Dobson circulation as well as upper stratosphere cooling) might affect changes in tropospheric height and temperature. All these topics merit future investigation.

ACKNOWLEDGEMENTS

S.H. is supported by the Scripps Institutional Postdoctoral Program Fellowship. G.K.V. is supported by the Leverhulme Trust, NERC and the Royal Society under a Wolfson Research Award. This work was begun at the Geophysical Fluid Dynamics program at Woods Hole Oceanographic Institution and we acknowledge all present for a stimulating atmosphere. We also thank two anonymous reviewers for their helpful and constructive comments.

APPENDIX: NUMERICAL SOLUTION OF THE TROPOPAUSE MODEL

In this section, we provide more details on how the height of the tropopause is solved numerically. We will start with the case that has a specified stratospheric dynamical heating profile Q_s and then discuss the special case with a radiative equilibrium stratosphere (i.e., $Q_s = 0$), which is used for the main body of our study. For clarity of the discussion, in a few places we repeat some of the equations that are already shown in the main text.

We assume a grey atmosphere that is transparent to solar radiation and write the infrared longwave radiative transfer equations as

$$\frac{\partial D}{\partial \tau} = B - D, \quad \frac{\partial U}{\partial \tau} = U - B. \quad (\text{A1})$$

D and U are downward and upward infrared irradiance, respectively, $B = \sigma T^4$ follows the Stefan–Boltzmann law, with $\sigma = 5.67 \times 10^{-8} \text{ W/m}^2$, and τ is optical depth, increasing downward. The upper boundary conditions (at the top of the atmosphere) are that $D = 0$ and $U = \text{OLR}$ at $\tau = 0$, and we take OLR to be given.

For ease of calculation, we define two variables, I and J , using linear combinations of U and D , as follows:

$$I = U - D, \quad J = U + D. \quad (\text{A2})$$

As a result, Equation A1 can be written as, equivalently,

$$\frac{\partial I}{\partial \tau} = J - 2B, \quad \frac{\partial J}{\partial \tau} = I. \quad (\text{A3})$$

The upper boundary conditions thus become $I = \text{OLR}$ and $J = \text{OLR}$ at $\tau = 0$. We assume radiative–dynamical equilibrium in the upper atmosphere, that is, the net convergence of the infrared radiation is balanced by the dynamical cooling induced by the stratospheric circulation,

$$\frac{\partial I}{\partial \tau} + Q_s = 0. \quad (\text{A4})$$

Using Equation A4 and the upper boundary condition, we compute the vertical profile of I ,

$$I = \text{OLR} - \overline{Q}_s, \quad (\text{A5})$$

where $\overline{Q}_s(\tau) = \int_0^\tau Q_s d\tau'$. Combining Equations A5 and A3, we get the vertical profile of J ,

$$J = (\tau + 1) \text{OLR} - \overline{\overline{Q}}_s, \quad (\text{A6})$$

and the vertical profile of B ,

$$B = \left(\frac{\tau + 1}{2}\right) \text{OLR} + \frac{Q_s - \overline{\overline{Q}}_s}{2}, \quad (\text{A7})$$

where $\overline{\overline{Q}}_s(\tau) = \int_0^\tau \overline{Q}_s d\tau'$. Using the Stefan–Boltzmann law, we get the radiative–dynamical equilibrium temperature profile,

$$T_{\text{rde}} = \left[\left(\frac{\tau + 1}{2\sigma}\right) \text{OLR} + \frac{Q_s - \overline{\overline{Q}}_s}{2\sigma} \right]^{1/4}. \quad (\text{A8})$$

Note that the radiative–dynamical equilibrium temperature profile is derived without any lower boundary conditions at the surface. Combining Equations A2, A5, and A6, we have

the vertical profiles of U and D ,

$$U = \left(\frac{\tau + 2}{2}\right) \text{OLR} - \frac{\overline{Q}_s + \overline{\overline{Q}}_s}{2}, \quad D = \left(\frac{\tau}{2}\right) \text{OLR} + \frac{\overline{Q}_s - \overline{\overline{Q}}_s}{2}. \quad (\text{A9})$$

In this study, we prescribe the vertical profile of optical depth $\tau = \tau(z)$, which may consist of one or two infrared absorbers. We assume the exponential decrease of pressure with height $p = p_s \exp(-z/H_s)$, where surface pressure $p_s = 1,000 \text{ hPa}$ and the scale height of dry air $H_s = 8 \text{ km}$. Therefore, one can convert the vertical coordinates of τ , p , and z from one to another.

We assume that the lower atmosphere below the radiative–dynamical equilibrium layer, separated by the boundary at $z = H_T$, is uniformly stratified with a specified lapse rate Γ , namely,

$$T(z) = \begin{cases} T_{\text{rde}}(z), & z \geq H_T, \\ T_T + \Gamma(H_T - z), & H_T \geq z \geq 0, \end{cases} \quad (\text{A10})$$

where $T_T = T_{\text{rde}}|_{z=H_T}$. The lower boundary condition at the surface requires that $U = \sigma T_s^4$ at $z = 0$, where T_s is the surface temperature (no ground temperature jump). To summarize, with the specified OLR, Γ , $\tau(z)$, and $Q_s(z)$, the only unknown variable in the system is the tropopause height H_T . Therefore, we can solve the system numerically by iterating over the different values of H_T until the lower boundary condition is matched. Note that the numerical solution of H_T should be interpreted literally as the boundary between the upper radiative–dynamical equilibrium layer and the lower uniformly stratified layer, but not the tropopause height; see section 5 for an illustrative example.

In the main body of this study, our tropopause model does not involve the stratospheric dynamical heating and, in other words, Q_s vanishes. In that case, we have radiative equilibrium solutions instead for the upper atmosphere, that is,

$$D, U, B = \left(\frac{\tau}{2}, \frac{\tau + 2}{2}, \frac{\tau + 1}{2}\right) \text{OLR}, \quad (\text{A11})$$

and

$$T_{\text{re}} = \left[\left(\frac{\tau + 1}{2\sigma}\right) \text{OLR} \right]^{1/4}. \quad (\text{A12})$$

In our two-band model, we have two downward and two upward infrared irradiances (D^{lw} , D^{win} , U^{lw} , and U^{win}), instead of one each as in our grey model (D and U). We also have five boundary conditions ($D^{\text{lw}} = 0$, $D^{\text{win}} = 0$, $U^{\text{lw}} + U^{\text{win}} = \text{OLR}$ at the top of atmosphere, and $U^{\text{lw}} = \beta \sigma T_s^4$ and $U^{\text{win}} = (1 - \beta) \sigma T_s^4$ at the surface) instead of three ($D = 0$ and $U = \text{OLR}$ at the top of atmosphere, and $U = \sigma T_s^4$ at the surface). Thus, the system is still

closed and the height of the tropopause can be solved numerically using an iterative method similar to that used in the grey scheme.

REFERENCES

- Andrews, D.G. (2010) *An Introduction to Atmospheric Physics*. ISBN 978-0521693189. Cambridge, UK: Cambridge University Press.
- Arrhenius, S. (1896) On the influence of carbonic acid in the air upon the temperature of the ground. *Philosophical Magazine*, 41, 237–276.
- Austin, J. and Reichler, T.J. (2008) Long-term evolution of the cold point tropical tropopause: simulation results and attribution analysis. *Journal of Geophysical Research: Atmospheres*, 113, D00B10.
- Birner, T. (2010) Residual circulation and tropopause structure. *Journal of the Atmospheric Sciences*, 67(8), 2582–2600.
- Danielsen, E.F. (1968) Stratospheric–tropospheric exchange based on radioactivity, ozone and potential vorticity. *Journal of the Atmospheric Sciences*, 25(3), 502–518.
- Emanuel, K., Solomon, S., Folini, D., Davis, S. and Cagnazzo, C. (2013) Influence of tropical tropopause layer cooling on atlantic hurricane activity. *Journal of Climate*, 26(7), 2288–2301.
- Frierson, D.M., Held, I.M. and Zurita-Gotor, P. (2006) A gray-radiation aquaplanet moist GCM. Part I: static stability and eddy scale. *Journal of the Atmospheric Sciences*, 63(10), 2548–2566.
- Fueglistaler, S., Legras, B., Beljaars, A., Morcrette, J.J., Simmons, A., Tompkins, A. and Uppala, S. (2009) The diabatic heat budget of the upper troposphere and lower/mid stratosphere in ECMWF reanalyses. *Quarterly Journal of the Royal Meteorological Society*, 135(638), 21–37.
- Geen, R., Czaja, A. and Haigh, J.D. (2016) The effects of increasing humidity on heat transport by extratropical waves. *Geophysical Research Letters*, 43(15), 8314–8321.
- Goody, R. (1964) *Atmospheric Radiation: Theoretical Basis*, Vol. 1. Oxford: Clarendon.
- Haqq-Misra, J., Lee, S. and Frierson, D.M. (2011) Tropopause structure and the role of eddies. *Journal of the Atmospheric Sciences*, 68(12), 2930–2944.
- Hartmann, D.L. and Larson, K. (2002) An important constraint on tropical cloud-climate feedback. *Geophysical Research Letters*, 29(20), 12–11.
- Held, I.M. (1982) On the height of the tropopause and the static stability of the troposphere. *Journal of the Atmospheric Sciences*, 39(2), 412–417.
- Held, I.M. and Soden, B.J. (2000) Water vapor feedback and global warming. *Annual Review of Energy and the Environment*, 25(1), 441–475.
- Highwood, E. and Hoskins, B. (1998) The tropical tropopause. *Quarterly Journal of the Royal Meteorological Society*, 124(549), 1579–1604.
- Holton, J.R., Haynes, P.H., McIntyre, M.E., Douglass, A.R., Rood, R.B. and Pfister, L. (1995) Stratosphere–troposphere exchange. *Reviews of Geophysics*, 33(4), 403–439.
- Huang, X., Chen, X., Soden, B.J. and Liu, X. (2014) The spectral dimension of longwave feedback in the CMIP3 and CMIP5 experiments. *Geophysical Research Letters*, 41(22), 7830–7837.
- Juckes, M. (2000) The static stability of the midlatitude troposphere: the relevance of moisture. *Journal of the Atmospheric Sciences*, 57(18), 3050–3057.
- Kim, J., Grise, K.M. and Son, S.W. (2013) Thermal characteristics of the cold-point tropopause region in CMIP5 models. *Journal of Geophysical Research: Atmospheres*, 118(16), 8827–8841.
- Kuang, Z. and Hartmann, D.L. (2007) Testing the fixed anvil temperature hypothesis in a cloud-resolving model. *Journal of Climate*, 20(10), 2051–2057.
- Li, Y., Yang, P., North, G.R. and Dessler, A. (2012) Test of the fixed anvil temperature hypothesis. *Journal of the Atmospheric Sciences*, 69(7), 2317–2328.
- Lin, P., Paynter, D., Ming, Y. and Ramaswamy, V. (2017) Changes of the tropical tropopause layer under global warming. *Journal of Climate*, 30(4), 1245–1258.
- Lorenz, D.J. and DeWeaver, E.T. (2007) Tropopause height and zonal wind response to global warming in the IPCC scenario integrations. *Journal of Geophysical Research: Atmospheres*, 112, D10119.
- Lu, J., Chen, G. and Frierson, D.M. (2008) Response of the zonal mean atmospheric circulation to El Niño versus global warming. *Journal of Climate*, 21(22), 5835–5851.
- Manabe, S. and Strickler, R.F. (1964) Thermal equilibrium of the atmosphere with a convective adjustment. *Journal of the Atmospheric Sciences*, 21(4), 361–385.
- Marchand, R., Ackerman, T., Smyth, M. and Rossow, W.B. (2010) A review of cloud top height and optical depth histograms from MISR, ISCCP, and MODIS. *Journal of Geophysical Research: Atmospheres*, 115, D16206.
- Mokhov, I. and Akperov, M. (2006) Tropospheric lapse rate and its relation to surface temperature from reanalysis data. *Izvestiya, Atmospheric and Oceanic Physics*, 42(4), 430–438.
- Mote, P.W., Rosenlof, K.H., McIntyre, M.E., Carr, E.S., Gille, J.C., Holton, J.R., Kinnerson, J.S., Pumphrey, H.C., Russell, J.M. and Waters, J.W. (1996) An atmospheric tape recorder: the imprint of tropical tropopause temperatures on stratospheric water vapor. *Journal of Geophysical Research: Atmospheres*, 101(D2), 3989–4006.
- O’Gorman, P.A. and Schneider, T. (2008) The hydrological cycle over a wide range of climates simulated with an idealized GCM. *Journal of Climate*, 21(15), 3815–3832.
- Santer, B.D., Wehner, M.F., Wigley, T.M.L., Sausen, R., Meehl, G.A., Taylor, K.E., Ammann, C., Arblaster, J., Washington, W.M., Boyle, J.S. and Brüggemann, W. (2003) Contributions of anthropogenic and natural forcing to recent tropopause height changes. *Science*, 301(5632), 479–483.
- Schneider, T. (2004) The tropopause and the thermal stratification in the extratropics of a dry atmosphere. *Journal of the Atmospheric Sciences*, 61(12), 1317–1340.
- Seeley, J.T., Jeevanjee, N. and Romps, D.M. (2019) FAT or FiTT: are anvil clouds or the tropopause temperature-invariant?. *Geophysical Research Letters*, 46(3), 1842–1850.
- Simpson, G.C. (1928) Further studies in terrestrial radiation. *Memoirs of the Royal Meteorological Society*, III(21), 322–323.
- Stone, P.H. and Carlson, J.H. (1979) Atmospheric lapse rate regimes and their parametrization. *Journal of the Atmospheric Sciences*, 36(3), 415–423.
- Thompson, D.W., Bony, S. and Li, Y. (2017) Thermodynamic constraint on the depth of the global tropospheric circulation. *Proceedings of the National Academy of Sciences of the United States of America*, 114(31), 8181–8186.
- Thuburn, J. and Craig, G.C. (1997) GCM tests of theories for the height of the tropopause. *Journal of the Atmospheric Sciences*, 54(7), 869–882.

- Thuburn, J. and Craig, G.C. (2000) Stratospheric influence on tropopause height: the radiative constraint. *Journal of the Atmospheric Sciences*, 57(1), 17–28.
- Vallis, G.K. (2017) *Atmospheric and Oceanic Fluid Dynamics: Fundamentals and Large-Scale Circulation*, 2nd edn. Cambridge, UK: Cambridge University Press.
- Vallis, G.K., Colyer, G., Geen, R., Gerber, E., Jucker, M., Maher, P., Paterson, A., Pietschnig, M., Penn, J. and Thomson, S.I. (2018) Isca, v1.0: a framework for the global modelling of the atmospheres of Earth and other planets at varying levels of complexity. *Geoscientific Model Development*, 11, 843–859. <https://doi.org/10.5194/gmd-11-843-2018>.
- Vallis, G.K., Zurita-Gotor, P., Cairns, C. and Kidston, J. (2015) Response of the large-scale structure of the atmosphere to global warming. *Quarterly Journal of the Royal Meteorological Society*, 141(690), 1479–1501.
- Wang, S., Camargo, S.J., Sobel, A.H. and Polvani, L.M. (2014) Impact of the tropopause temperature on the intensity of tropical cyclones: an idealized study using a mesoscale model. *Journal of the Atmospheric Sciences*, 71(11), 4333–4348.
- Weaver, C. and Ramanathan, V. (1995) Deductions from a simple climate model: factors governing surface temperature and atmospheric thermal structure. *Journal of Geophysical Research: Atmospheres*, 100(D6), 11585–11591.
- Wilcox, L., Hoskins, B. and Shine, K. (2012) A global blended tropopause based on ERA data. Part I: climatology. *Quarterly Journal of the Royal Meteorological Society*, 138(664), 561–575.
- World Meteorological Organization. (1957) Definition of the tropopause. *WMO Bulletin*, 6, 136.
- Zurita-Gotor, P. and Vallis, G.K. (2011) Dynamics of midlatitude tropopause height in an idealized model. *Journal of the Atmospheric Sciences*, 68(4), 823–838.
- Zurita-Gotor, P. and Vallis, G.K. (2013) Determination of extratropical tropopause height in an idealized gray radiation model. *Journal of the Atmospheric Sciences*, 70(7), 2272–2292.

How to cite this article: Hu S, Vallis GK. Meridional structure and future changes of tropopause height and temperature. *QJR Meteorol Soc.* 2019;145:2698–2717. <https://doi.org/10.1002/qj.3587>